Environmental pH signals the release of monosaccharides from cell wall in coral symbiotic alga

Yuu Ishii[1, 2], Hironori Ishii[1], Takeshi Kuroha[1]†, Ryusuke Yokoyama[1], Ryusaku Deguchi[2], Kazuhiko Nishitani[3], Jun Minagawa[4,5], Masakado Kawata[1], Shunichi Takahashi[6], Shinichiro Maruyama[1,7]*

[1] Department of Ecological Developmental Adaptability Life Sciences, Graduate School of Life Sciences, Tohoku University, Sendai, Miyagi, Japan

[2] Department of Biology, Miyagi University of Education, Sendai, Miyagi, Japan

[3] Department of Biological Sciences, Faculty of Science, Kanagawa University, Yokohama, Kanagawa, Japan

[4] Division of Environmental Photobiology, National Institute for Basic Biology, Okazaki, Aichi, Japan

[5] Department of Basic Biology, School of Life Science, SOKENDAI (The Graduate University for Advanced Studies), Okazaki, Aichi, Japan

[6] Tropical Biosphere Research Center, University of the Ryukyus, Motobu, Okinawa, Japan

[7] Graduate School of Humanities and Sciences, Ochanomizu University, Bunkyo-ku, Tokyo, Japan.

† Present address: Division of Crop Genome Editing, Institute of Agrobiological Sciences, National Agriculture and Food Research Organization (NARO), Tsukuba, Ibaraki, Japan.

*Corresponding author: Shinichiro Maruyama

Email: maruyama@tohoku.ac.jp

Abstract

Reef-building corals thrive in oligotrophic environments due to their possession of endosymbiotic algae. Confined to the low pH interior of the symbiosome within the cell, the algal symbiont provides the coral host with photosynthetically fixed carbon. However, it remains unknown how carbon is released from the algal symbiont for uptake by the host. Here we show, using cultured symbiotic dinoflagellate, *Breviolum* sp., that decreases in pH directly accelerates the release of monosaccharides, i.e., glucose and galactose, into the ambient environment. Under low pH conditions, the cell surface structures were deformed and genes related to cellulase were significantly upregulated in *Breviolum*. Importantly, the release of monosaccharides was suppressed by the cellulase inhibitor, glucopyranoside, linking the release of carbon to degradation of the agal cell wall. Our results suggest that the low pH signals the cellulase-mediated release of monosaccharides from the algal cell wall as an environmental response in coral reef ecosystems.

Main text

Introduction

Coral reef ecosystems are sustained by symbiosis between stony corals and marine dinoflagellates from the family Symbiodiniaceae, which are found in nature as free-living mixotrophs (Decelle et al., 2018; Jeong et al., 2012), as well as are primary producers in symbiotic relationships with various partners, including multicellular (e.g. Cnidaria, Mollusca, Porifera) and unicellular organisms (Foraminifera, Ciliates) (LaJeunesse et al., 2018). In oligotrophic oceans, transfer of atmospheric carbon photosynthetically fixed by the symbiotic algae to their hosts is a fundamental flux to sustain the growth and productivity of coral reef ecosystems.

Although it is generally accepted that Symbiodiniaceae algae provide photosynthates to their symbiotic partners, the molecular details are largely unknown (Falkowski et al., 1984; Ishii et al., 2019; Ishikura et al., 1999; Muscatine, 1990; Rahav et al., 1989; Stat et al., 2008; Whitehead and Douglas, 2003). Members of this family reside in an intracellular organelle called the ‘symbiosome’ within cnidarian host cells or in the extracellular ‘symbiotic tube’ systems of giant clams. These are thought to be special low pH environments that are acidified by V-type H^+-ATPase proton pumps (Armstrong et al., 2018; Barott et al., 2015; Davy et al., 2012). While low pH environments are stressors to algae in general, they can be beneficial when CO_2 uptake is encouraged by the hosts’ carbon-concentrating functions, enhancing photosynthesis (Armstrong et al., 2018; Barott et al., 2015). A previous study has demonstrated a photosynthesis-dependent glucose transfer from Symbiodiniaceae to sea anemone hosts (Burriesci et al., 2012), and some sugar transporters

are proposed to be involved in glucose transfer (Lehnert et al., 2014; Sproles et al., 2018). Other studies suggest that the amount of transfer is regulated by the C-N balance (Rädecker et al., 2021; Xiang et al., 2020). Nevertheless, the mechanism of algal glucose secretion is not yet characterized.

Results

To investigate the physiological effects of low pH, a characteristic environmental factor in symbioses, on algal intrinsic properties, a Symbiodiniaceae alga *Breviolum* sp. SSB01 (hereafter, *Breviolum*) was grown in a host-independent manner and cell proliferation and photosynthetic activities were measured. By comparing the growth rate of *Breviolum* in normal culture medium (pH 7.8) and acidic medium (pH 5.5, hereafter called "low pH"), we showed that the low pH medium considerably suppressed algal growth (Figure 1A) and culturing at low pH for one day resulted in significant declines in photosynthesis activity (Figure 1B).

Contrary to our expectation, the amount of glucose secreted into the culture medium was higher at low pH (Figure 1C) and the secreted galactose similarly showed an increasing trend (Figure 1D). These trends suggest that *Breviolum* is capable of secreting monosaccharides autonomously without host signals, and that low pH enhanced the secretion. On the addition of the photosynthesis inhibitor 3-(3,4-dichlorophenyl)-1,1-dimethylurea (DCMU), the concentrations of glucose and galactose in the medium increased (Supplementary Figure S1), suggesting the presence of a yet uncharacterized pathway (Burriesci et al., 2012).

To investigate the response of *Breviolum* to acidic environments at the morphological level, cells cultured in different media were examined by microscopy. *Breviolum* cells in low pH media were more spread out and less clustered than the cells in normal media (Figure 2A, B). Scanning electron microscope (SEM) observations revealed that many of the *Breviolum* cells cultured at low pH exhibited wrinkled structures on their cell surfaces (Figure 2C, D). Furthermore, transmission electron microscopy (TEM) revealed that the cell surface structures of the low pH media group were 'exfoliated' (Figure 2E, F). These suggest that low pH affects the structures and properties of a cellulosic cell wall found in coccoid Symbiodiniaceae cells (Colley and Trench, 1983; Markell et al., 1992).

To identify the mechanism involved in the monosaccharide secretion of *Breviolum*, we compared gene expression changes between the 'control vs normal' and 'control vs low pH' comparisons, and identified 3 and 4527 differentially expressed genes (DEGs), respectively (Figure 3A, Supplementary Dataset S1). The gene ontology (GO) term enrichment and KEGG pathway analysis of these two gene sets resulted in the detection of 0 (control vs. normal) and 16 (control vs. low pH) terms (Supplementary Dataset S2), which

included categories related to carbon metabolism (Figure 3B, Supplementary Figure S2). The CAZy database (Lombard et al., 2014) analysis showed that 12 DEGs (28 isoforms) were annotated with Carbohydrate-Active enZymes (CAZymes) activity (Figure 3C, Supplementary Dataset S3). One of the genes, TRINITY_DN40554_c2_g2, was shown to encode cellulase (exocrine cellulolytic enzyme) harbouring a signal peptide (Figure 3C) with high similarity to dinoflagellate homologs (Kwok and Wong, 2010) (Supplementary Figure S3).

To confirm the effect of cellulase on monosaccharide secretion, we examined whether secretions were inhibited by the cellulase inhibitor Para-nitrophenyl 1-thio-beta-d-glucopyranosid (PSG) (Figure 4). PSG inhibited the secretion of both glucose and galactose in a dose-dependent manner, suggesting that cell wall degradation by cellulase is involved in the secretion of monosaccharides from *Breviolum* cells.

Discussion

The transfer of photosynthetically fixed carbon from symbiotic algae to host cnidarians, including corals, is a cornerstone of their mutual symbiotic relationship (Muscatine, 1990). Unlike the current accepted model of monosaccharide secretion that assumes photosynthetically fixed carbon is directly exported from the algal symbiont via unidentified glucose transporter(s) (Lehnert et al., 2014; Sproles et al., 2018), our results suggest that stored carbon can be released from the algal cell wall as an environmental response. In the present study, we showed that a decrease in ambient pH, consistent with the interior pH of the symbiosome, accelerates the monosaccharide secretion from *Breviolum* (Figure 1). Importantly, this low pH-associated secretion was suppressed by inhibition of cellulase (Figure 4), suggesting that algal symbionts release monosaccharides into the symbiosome within host cnidarian cells by cell wall degradation. Previous studies showed that cell wall degradation/rearrangement by cellulase is required for cell cycle progression (Kwok and Wong, 2010) and cellulose synthesis is involved in morphogenesis (Chan et al., 2019) in dinoflagellates. Indeed, wrinkle and exfoliation of the algal cell wall was observed under low pH conditions using SEM and TEM, respectively (Figure 2). We need to note that our results do not deny the current accepted model, but rather suggest a multi-pathway hypothesis supported by the following observations: (i) the secretion of monosaccharides was not completely inhibited by cellulase inhibition, (ii) this new pathway occurred over days, compared to previous reports, where exported glucose was detectable in the host after only 30-60 minutes (Burriesci et al., 2012), (iii) in contrast to previous studies (Burriesci et al., 2012), DCMU did not suppress, but rather increased the secretion of monosaccharides over a longer time span (Supplementary Figure S1). Importantly, low pH upregulated the expression of genes associated with not only cellulase (Figure 3) but glycolysis probably fuelled by degradation of storage compound like starch (Supplementary Figure S2). This suggests the photosynthesis-limiting conditions trigger an

environmental response in the algae to sustain cell proliferation, through cell cycle progression by cellulase, accompanying cell wall degradation and monosaccharide secretion.

Like Symbiodiniaceae, some freshwater green algae are known to be symbiotic with a range of hosts. A number of *Chlorella* strains, with and without symbiotic ability, autonomously secrete monosaccharides under low pH conditions via unknown mechanisms (Kessler et al., 1991; Mews and Smith, 1982). The monosaccharides include maltose and, to a lesser extent, glucose (Arriola et al., 2018). Dinoflagellates are also known to secrete viscous substances, including monosaccharides, as an environmental response, likely for cell aggregation and biofilm formation (Mandal et al., 2011). Thus, secretion of monosaccharides appears to be a fairly conserved environmental response and may be to compensate for retarded cell cycle progression. Therefore, acidifying symbiosomes may be an evolutionary successful strategy for cnidarian hosts to promote environmental responses of algal symbionts, which enables monosaccharides to be efficiently secreted within the organelle.

Generally, within ecosystems energy is transferred from photosynthetic primary producer to consumer by predation. Uniquely, in coral reef ecosystems energy is mainly transported from algae to corals after establishing a symbiotic relationship (Davy et al., 2012). Thus, understanding its mechanism has wider implications to understanding how energy is shared over the entire coral reef ecosystem. The multi-pathway hypothesis we propose here entails the direct transfer of photosynthates via glucose transporter(s) on their cell membrane (Lehnert et al., 2014; Sproles et al., 2018) as well as monosaccharide secretion following cell wall degradation. It remains to be determined how much each pathway contributes to the energy supply of host. However, since one pathway uses de novo photosynthates and the other uses stored photosynthates, combined they might allow for a stable supply of energy to the host, e.g., over the entire light/dark day cycle, and under photosynthesis-limiting conditions like environmental stress or cloudy days where the cellulose-related pathway could be of substantial importance. Although genetic transformation for Symbiodiniaceae is unavailable yet (Chen et al., 2019), knock-down of the cellulase gene will bring a clue to test this. Overall, our study provides a new insight into how carbon is provided by symbiotic algae to the coral reef ecosystem.

Materials and Methods

Strains and culture conditions

We obtained the *Breviolum* (formerly *Symbiodinium* clade B) strain SSB01, an axenic uni-algal strain closely related to the genome-sequenced strain *B. minutum* Mf1.05b (clade B), as a generous gift from Profs. John R. Pringle and Arthur R. Grossman (Shoguchi et al., 2013; Xiang et al., 2013). The *Breviolum* was maintained according to previous study (Ishii et al., 2018). Stock cultures were incubated at 25°C in

171 medium containing 33.5 g/L of Marine Broth (MB) (Difco Laboratories, New Jersey, USA), 250 mg/L of
172 Daigo's IMK Medium (Nihon Pharmaceutical, Japan), and PSN (Gibco, Thermo Fisher Scientific,
173 Massachusetts, USA), with final concentrations of penicillin, streptomycin, and neomycin at 0.01, 0.01, and
174 0.02 mg/mL, respectively. Light was provided at an irradiance of approximately 100 µmol photons/m^2s in a
175 12 h light:12 h dark cycle. In experiments, IMK medium containing 33.5 g/L of sea salt (Sigma-Aldrich,
176 Merck Millipore, Germany), 250 mg/L of Daigo's IMK Medium, and PSN with final concentrations of
177 penicillin, streptomycin, and neomycin at 0.01, 0.01, and 0.02 mg/mL, respectively, was used. The pH of
178 this medium was adjusted to 5.5 using HCl for the low pH experiments.
179
180 **Sample preparation for Ion chromatography, RNAseq, and electron microscopy**
181 The incubation conditions were designed to allow detection of changes in the early phases of low pH
182 stimulus responses. Prior to exposure to low pH conditions, *Breviolum* cultures were incubated for one
183 week in IMK medium at densities of 8×10^6 cells/20 mL in T25 culture flasks with a filter cap (TrueLine
184 Cell Culture Flasks, TR6000) under a light-dark cycle. During experiments, *Breviolum* was cultured in two
185 kinds of media: normal (pH 7.8) and low pH (pH 5.5), for 24 h (12 h light:12 h dark), starting at densities
186 of 8×10^6 cells/20 mL per T25 culture flask, placed at randomized positions. DCMU was dissolved in
187 ethanol at the concentration of 20 mM and was added to cultures to a final concentration of 20 µM. The
188 cultured cells were collected by centrifugation at 2,000 × g for 5 min at room temperature. The cells were
189 then used for RNA-seq and electron microscopy, and the supernatants were used for ion chromatographic
190 determination.
191
192 **Ion chromatography**
193 Samples (n = 4 biological replicates) of the supernatant from the control (0 h), normal (24 h) and low pH
194 (24 h) cultures were filtered using a 0.22 µm PVDF filter (Merck Millipore, Germany). These samples were
195 loaded onto an OnGuard column (Dionex OnGuard II Cartridge) (Thermo Scientific) to remove the
196 sulphate and halogen, according to the manufacturer's instructions. The samples were quantified using
197 high-performance anion-exchange chromatography with pulsed amperometric detection (HPAEC-PAD)
198 using a Dionex ICS-5000 system equipped with a CarboPac PA1 column (Dionex) (Shinohara et al., 2017).
199 The column was operated at a flow rate of 1.1 mL/min with the following phases: (1) a linear gradient of 0–
200 100 mM NaOH from 0 to 31 min, (2) a linear gradient of 0–150 mM sodium acetate containing 100 mM
201 NaOH from 31 to 34 min, and (3) an isocratic 150 mM sodium acetate/100 mM NaOH from 34 to 41 min.
202 Myo-inositol (2 µg/mL) was added to each sample as an internal standard for quantification.
203 The concentrations of monosaccharides were calculated by comparing the peak ratios between the targets
204 of interest and standards. The secreted amounts were calculated by subtracting the concentrations on day 0
205 from those of day 1.
206

207 **Growth rate, photosynthesis, and respiratory activity assay**

208 To measure growth rate (n = 6 biological replicates), photosynthesis and respiratory activities (n = 4
209 biological replicates), *Breviolum* cultures were incubated in normal IMK media for one week and
210 subsequently changed to fresh normal or low pH IMK media. Growth rate comparisons between the normal
211 and low pH media conditions were conducted using 100 µL of media (625 cells/µL) in a 96-well plate. Cell
212 growth was monitored by measuring the optical density at 730 nm (OD730) of the liquid cultures using a
213 Multiskan GO microplate spectrophotometer (Thermo Fisher Scientific, Massachusetts, USA).
214 Photosynthesis and respiratory activities were determined using cultures at densities of 1×10^6 cells/mL in
215 fresh normal and low pH media, on days 0 and 1 after changing the medium, separate from the
216 transcriptome analysis. Respiration rates were calculated using the dark-phase oxygen consumption rates
217 and photosynthesis rates were calculated by subtracting the respiration rates from the light-phase oxygen
218 evolution rates. Mean estimates with standard errors were calculated from single measurements of four
219 different cultures per medium condition.

220

221 **RNA extraction and sequencing**

222 Four samples (n = 4 biological replicates) from each of the control (day 0), normal (day 1), or low pH (day
223 1) cultures were added to 500 µL of TRIZOL reagent (Thermo Fisher Scientific, Massachusetts, USA) and
224 stored at -80 °C. The samples were ground with two sizes of glass beads (20 µL volume each of '≤106 µm'
225 and '425–600 µm') (Sigma-Aldrich, Merck Millipore, Germany) using a vortex and performing 5 cycles of
226 freezing and thawing with a -80˚C freezer. RNA extraction with TRIZOL reagent and a high salt solution
227 for precipitation (plant) (Takara Bio, Japan) was conducted according to the manufacturer's instructions.
228 The quality and quantity of the RNA was verified using an Agilent RNA 6000 Nano Kit on an Agilent
229 Bioanalyzer (Agilent Technologies, California, USA) and a Nanodrop spectrophotometer (Thermo Fisher
230 Scientific, Massachusetts, USA), respectively. Total RNA samples were subjected to library preparation
231 using an NEB Next Ultra RNA Library Prep Kit (New England Biolabs, Ipswich, MA, USA) according to
232 the manufacturer's protocol (NEB #E7530). These mRNA libraries were sequenced in an Illumina
233 NovaSeq6000 (S2 flow cell) in dual flow cell mode with 150-mer paired-end sequences (Filgen Inc.,
234 Japan). The raw read data were submitted to DDBJ/EMBL-EBI/GenBank under the BioProject accession
235 number PRJDB12295.

236

237 **Transcriptome analysis**

238 A total of 12 libraries were obtained, trimmed, and filtered using the trimmomatic option of the Trinity
239 program. Paired output reads were used for analysis, and de novo assembly was performed using the
240 Trinity program (Grabherr et al., 2011) to obtain the transcript sequences. The reads from each library were
241 mapped onto the de novo assembly sequences and read count data, and the transcripts per million (TPM)
242 were calculated using RSEM (Li and Dewey, 2011) with bowtie2 (Langmead and Salzberg, 2012).

243
244 In this study, RNA-seq produced 550,711,174 reads from the 12 samples (four independent culture flasks
245 under three conditions), yielding 239,047 contigs by de novo assembly using Trinity. The total number of
246 mapped reads of the quadruplicates in the de novo assembled transcriptome dataset were 77,160,394 reads
247 for samples taken before medium change (labelled as 'control'), 74,594,446 for the normal pH culture
248 condition (labelled as 'normal'), and 73,882,605 for the low pH culture condition (labelled as 'lowpH').
249 Overall, we obtained the count values of the genes in the transcriptome dataset under the three conditions.
250 Differential gene expression analysis was conducted using the count data as inputs for the R package TCC
251 (Sun et al., 2013) to compare the tag count data with robust normalization strategies, with an option using
252 edgeR (Robinson et al., 2010) to detect differential expressions implemented in TCC. To identify the
253 DEGs, a false discovery rate (FDR, or q-value) of 0.01, was used as the cutoff.
254
255 To annotate the de novo transcript sequences, BLASTp search was performed (E-value cutoff, 10^{-4}) against
256 the GenBank *nr* database using all the transcript sequences as queries, resulting in 51,833 orthologs. Gene
257 ontology (GO) term annotation of the de novo transcript sequences was performed using InterProScan
258 (Jones et al., 2014) ver 5.42-78.0, resulting in 7,336 genes with GO terms. GO term enrichment analysis
259 was performed using the GOseq (Young et al., 2010) package in R. Overrepresented p-values produced by
260 GOseq were adjusted using the Benjamini-Hochberg correction (Benjamini and Hochberg, 1995). An
261 adjusted p-value (q-value) of 0.05, was used to define enriched GO terms. In the KEGG pathway analysis,
262 the ortholog protein sequence obtained via BLASTp search of the DEGs was used as a query. Additionally,
263 KOID was added by blastKOALA (Kanehisa et al., 2016) (https://www.kegg.jp/blastkoala/) and mapped to
264 the KEGG pathway using KEGmappar (Kanehisa and Sato, 2020)
265 (https://www.genome.jp/kegg/mapper.html). For CAZome analysis, all isoform sequences of the DEGs
266 were analysed using CAZy (Lombard et al., 2014) (http://www.cazy.org/).
267
268 **Cellulase inhibition experiment**
269 *Breviolum* cells cultured in IMK for more than 1 week were transferred to 24 well plates at 4×10^6 cells/ml
270 density and incubated for 24 h (12 h light:12 h dark) in IMK medium containing 0, 0.1, and 1 mM PSG (n
271 = 4 biological replicates for each condition). The supernatant from each culture was collected following
272 centrifugation at 2,000 × g for 2 min at room temperature. The medium samples were filtered using a 0.22
273 µm PVDF filter (Merck Millipore, Germany).
274 Glucose and galactose were quantified using a LC–MS/MS system in which a Shimadzu UPLC system
275 (Shimadzu, Kyoto, Japan) was interfaced to an AB Sciex QTrap 5500 mass spectrometer equipped with an
276 electrospray ionization source (AB SCIEX, Foster, CA, USA). A UK-Amino column (3 µm, 2.1 mm × 250
277 mm, Imtakt Corporation, Kyoto, Japan) was applied for analysis. Mobile phase A is 0.1% formic acid, and
278 mobile phase B is acetonitrile. Samples (1 µl) were injected and analyzed over a gradient of: 0–0.5 min

95% buffer B (isocratic); 0.5–10 min 85% buffer B (linearly decreasing); 10–15 min 40% buffer B (linear decreasing). The column was equilibrated for 5 min before each sample injection. The flow rate was 0.3 ml/min. Under these analytical conditions, the retention times for glucose and galactose were 11.6 and 10.9 minutes, respectively. Mass spectrometric analysis employed electrospray ionization in the negative mode with multiple reaction monitoring (MRM) at the transitions of m/z 179→89 for glucose and galactose. The optimized MS parameters were as follows: ion spray voltage (-4500V), declustering potential (-90V), entrance potential (-10V), collision energy (-12V), collision exit potential (-11V), collision gas (N2 gas) and nebulizer temperature (450 ◦C). Raw data was analyzed using MultiQuant software (AB SCIEX, Foster, CA, USA). Concentrations of monosaccharides were calculated by comparing the peak ratios between the targets of interest and standards.

Microscopy

To compare the cell conditions between the normal and low pH media, *Breviolum* was cultured and incubated for 3 weeks (12 h light:12 h dark) starting at densities of 1.6×10^7 cells/20 mL per T25 culture flask. Cell photos were taken using a TC20 automated cell counter (Bio-Rad Laboratories, Hercules, CA), and the numbers of cells adjacent to and isolated from other cells were randomly counted (853 and 664 cells pooled form n = 3 biological replicates were scored in the normal and low pH conditions, respectively). The cells were fixed in a DMSO:KOH (1:1) solution, stained with 10 mg/mL calcofluor white solution in Milli-Q water, and observed under an inverted microscope (Leica DMI6000 B).

For SEM, cells were fixed in 2% glutaraldehyde and 2% osmium (VIII) oxide, dehydrated with ethanol, and dried using the critical point drying technique. The samples were coated with osmium plasma and observed under a JSM-7500F microscope at 5 kV. The surface patterns of the cells were manually scored and classified as 'smooth' or 'wrinkled' (73 and 129 cells pooled form n = 4 technical replicates were blindly scored under the normal and low pH conditions, respectively). For TEM observation, the samples were dehydrated with ethanol and embedded in EPON812 polymerized with epoxy resin. Sections 80–90 nm thick were cut, coated with evaporated carbon for stabilisation, and stained with uranyl acetate and lead citrate. The sections were then imaged at 100 kV using a HITACHI H-7600 transmission electron microscope. The cells were then categorized as NP (non-peeled), P (peeled) or CP (completely-peeled) (181 and 166 cells pooled form n = 10 technical replicates were blindly scored under normal and low pH conditions, respectively).

Acknowledgments

We thank Drs. Naoki Shinohara and Fukumatsu Iwahashi for their support in ion chromatography and mass spectrometry, Ms Yuna Uchida for her assistance in maintaining the algal cultures, Dr. Sara E. Milward for her critical reading of the manuscript, Prof. Hiromu Tanimoto and Dr. Vladimiros Thoma for their help in preparing the manuscript, Drs. Kota Kera and Seiji Kojima for their contributions in the initial phase of the

project, as well as Profs. John R. Pringle and Arthur R. Grossman for their generous gift of algal cultures. This work was supported by JSPS KAKENHI (Grant Numbers JP20J01658 [to Y.I.], JP17K15163, JP19H04713 and JP19K06786 [to S.M.]), NIBB Collaborative Research Program 18-321 and 19-332 (to S.M.), Institute for Fermentation, Osaka (to S.M.), Program for Creation of Interdisciplinary Research, Frontier Research Institute for Interdisciplinary Sciences, Tohoku University (to S.M.), and the Gordon & Betty Moore Foundation's Marine Microbiology Initiative #4985 (to J.M.). Computational resources were provided by the Data Integration and Analysis Facility at the National Institute for Basic Biology and the NIG supercomputer at the ROIS National Institute of Genetics.

Competing Interests

Authors declare that they have no competing interests.

References

Armstrong EJ, Roa JN, Stillman JH, Tresguerres M. 2018. Symbiont photosynthesis in giant clams is promoted by V-type H+-ATPase from host cells. *J Exp Biol* **221**. doi:10.1242/jeb.177220

Arriola MB, Velmurugan N, Zhang Y, Plunkett MH, Hondzo H, Barney BM. 2018. Genome sequences of *Chlorella sorokiniana* UTEX 1602 and *Micractinium conductrix* SAG 241.80: implications to maltose excretion by a green alga. *Plant J* **93**:566–586. doi:10.1111/tpj.13789

Barott KL, Venn AA, Perez SO, Tambutté S, Tresguerres M. 2015. Coral host cells acidify symbiotic algal microenvironment to promote photosynthesis. *Proc Natl Acad Sci USA* **112**:607–612. doi:10.1073/pnas.1413483112

Benjamini Y, Hochberg Y. 1995. Controlling the false discovery rate: A practical and powerful approach to multiple testing. *J R Stat Soc, Ser B, Methodol (Online)* **57**:289–300. doi:10.1111/j.2517-6161.1995.tb02031.x

Burriesci MS, Raab TK, Pringle JR. 2012. Evidence that glucose is the major transferred metabolite in dinoflagellate-cnidarian symbiosis. *J Exp Biol* **215**:3467–3477. doi:10.1242/jeb.070946

Chan WS, Kwok ACM, Wong JTY. 2019. Knockdown of Dinoflagellate Cellulose Synthase *CesA1* Resulted in Malformed Intracellular Cellulosic Thecal Plates and Severely Impeded Cyst-to-Swarmer Transition. *Front Microbiol* **10**. doi:10.3389/fmicb.2019.00546

Chen JE, Barbrook AC, Cui G, Howe CJ, Aranda M. 2019. The genetic intractability of *Symbiodinium microadriaticum* to standard algal transformation methods. *PLOS ONE* **14**:e0211936. doi:10.1371/journal.pone.0211936

Colley NJ, Trench RK. 1983. Selectivity in phagocytosis and persistence of symbiotic algae by the scyphistoma stage of the jellyfish *Cassiopeia xamachana*. *Proceedings of the Royal Society of London Series B Biological Sciences* **219**:61–82. doi:10.1098/rspb.1983.0059

Davy SK, Allemand D, Weis VM. 2012. Cell biology of cnidarian-dinoflagellate symbiosis. *Microbiol Mol Biol Rev* **76**:229–261. doi:10.1128/MMBR.05014-11

Decelle J, Carradec Q, Pochon X, Henry N, Romac S, Mahé F, Dunthorn M, Kourlaiev A, Voolstra CR, Wincker P, de Vargas C. 2018. Worldwide occurrence and activity of the reef-building coral symbiont *Symbiodinium* in the open ocean. *Curr Biol* **28**:3625-3633.e3. doi:10.1016/j.cub.2018.09.024

Falkowski PG, Dubinsky Z, Muscatine L, Porter JW. 1984. Light and the bioenergetics of a symbiotic coral. *Bioscience* **34**:705–709. doi:10.2307/1309663

363 Grabherr MG, Haas BJ, Yassour M, Levin JZ, Thompson DA, Amit I, Adiconis X, Fan L, Raychowdhury
364 R, Zeng Q, Chen Z, Mauceli E, Hacohen N, Gnirke A, Rhind N, di Palma F, Birren BW, Nusbaum
365 C, Lindblad-Toh K, Friedman N, Regev A. 2011. Full-length transcriptome assembly from RNA-
366 Seq data without a reference genome. *Nat Biotechnol* **29**:644–652. doi:10.1038/nbt.1883
367 Ishii Y, Maruyama S, Fujimura-Kamada K, Kutsuna N, Takahashi S, Kawata M, Minagawa J. 2018.
368 Isolation of uracil auxotroph mutants of coral symbiont alga for symbiosis studies. *Sci Rep* **8**:3237.
369 doi:10.1038/s41598-018-21499-3
370 Ishii Y, Maruyama S, Takahashi H, Aihara Y, Yamaguchi T, Yamaguchi K, Shigenobu S, Kawata M, Ueno
371 N, Minagawa J. 2019. Global shifts in gene expression profiles accompanied with environmental
372 changes in cnidarian-dinoflagellate endosymbiosis. *G3-GENES GENOM GENET* **9**:2337–2347.
373 doi:10.1534/g3.118.201012
374 Ishikura M, Adachi K, Maruyama T. 1999. Zooxanthellae release glucose in the tissue of a giant clam,
375 *Tridacna crocea*. *Mar Biol* **133**:665–673. doi:10.1007/s002270050507
376 Jeong HJ, Yoo YD, Kang NS, Lim AS, Seong KA, Lee SY, Lee MJ, Lee KH, Kim HS, Shin W, Nam SW,
377 Yih W, Lee K. 2012. Heterotrophic feeding as a newly identified survival strategy of the
378 dinoflagellate *Symbiodinium*. *Proc Natl Acad Sci USA* **109**:12604–12609.
379 doi:10.1073/pnas.1204302109
380 Jones P, Binns D, Chang H-Y, Fraser M, Li W, McAnulla C, McWilliam H, Maslen J, Mitchell A, Nuka G,
381 Pesseat S, Quinn AF, Sangrador-Vegas A, Scheremetjew M, Yong S-Y, Lopez R, Hunter S. 2014.
382 InterProScan 5: genome-scale protein function classification. *Bioinformatics* **30**:1236–1240.
383 doi:10.1093/bioinformatics/btu031
384 Kanehisa M, Sato Y. 2020. KEGG Mapper for inferring cellular functions from protein sequences. *Protein*
385 *Sci* **29**:28–35. doi:10.1002/pro.3711
386 Kanehisa M, Sato Y, Morishima K. 2016. BlastKOALA and GhostKOALA: KEGG tools for functional
387 characterization of genome and metagenome sequences. *J Mol Biol* **428**:726–731.
388 doi:10.1016/j.jmb.2015.11.006
389 Kessler E, Kauer G, Rahat M. 1991. Excretion of sugars by *Chlorella* species capable and incapable of
390 symbiosis with *Hydra viridis*. *Bot Acta* **104**:58–63. doi:10.1111/j.1438-8677.1991.tb00194.x
391 Kwok ACM, Wong JTY. 2010. The activity of a wall-bound cellulase is required for and is coupled to cell
392 cycle progression in the dinoflagellate *Crypthecodinium cohnii*. *Plant Cell* **22**:1281–1298.
393 doi:10.1105/tpc.109.070243
394 LaJeunesse TC, Parkinson JE, Gabrielson PW, Jeong HJ, Reimer JD, Voolstra CR, Santos SR. 2018.
395 Systematic revision of Symbiodiniaceae highlights the antiquity and diversity of coral
396 endosymbionts. *Curr Biol* **28**:2570-2580.e6. doi:10.1016/j.cub.2018.07.008
397 Langmead B, Salzberg SL. 2012. Fast gapped-read alignment with Bowtie 2. *Nat Methods* **9**:357–359.
398 doi:10.1038/nmeth.1923
399 Lehnert EM, Mouchka ME, Burriesci MS, Gallo ND, Schwarz JA, Pringle JR. 2014. Extensive differences
400 in gene expression between symbiotic and aposymbiotic cnidarians. *G3-GENES GENOM GENET*
401 **4**:277–295. doi:10.1534/g3.113.009084
402 Li B, Dewey CN. 2011. RSEM: accurate transcript quantification from RNA-Seq data with or without a
403 reference genome. *BMC Bioinformatics* **12**:323. doi:10.1186/1471-2105-12-323
404 Lombard V, Golaconda Ramulu H, Drula E, Coutinho PM, Henrissat B. 2014. The carbohydrate-active
405 enzymes database (CAZy) in 2013. *Nucleic Acids Res* **42**:D490-495. doi:10.1093/nar/gkt1178
406 Mandal SK, Singh RP, Patel V. 2011. Isolation and characterization of exopolysaccharide secreted by a
407 toxic dinoflagellate, *Amphidinium carterae* Hulburt 1957 and its probable role in harmful algal
408 blooms (HABs). *Microb Ecol* **62**:518–527. doi:10.1007/s00248-011-9852-5
409 Markell D, Trench RK, Iglesias-Prieto R. 1992. Macromolecules associated with the cell walls of symbiotic
410 dinoflagellates. *Symbiosis* **12**:19–31.
411 Mews LK, Smith DC. 1982. The green hydra symbiosis. VI. What is the role of maltose transfer from alga
412 to animal? *Proc Royal Soc B* **216**:397–413. doi:10.1098/rspb.1982.0083
413 Muscatine L. 1990. The role of symbiotic algae in carbon and energy flux in reef corals. *Coral Reefs*
414 **25**:75–87.

415 Rädecker N, Pogoreutz C, Gegner HM, Cárdenas A, Roth F, Bougoure J, Guagliardo P, Wild C, Pernice M,
416 Raina J-B, Meibom A, Voolstra CR. 2021. Heat stress destabilizes symbiotic nutrient cycling in
417 corals. *Proc Natl Acad Sci USA* **118**:e2022653118. doi:10.1073/pnas.2022653118
418 Rahav O, Dubinsky Z, Achituv Y, Falkowski PG. 1989. Ammonium metabolism in the zooxanthellate
419 coral, *Stylophora pistillata*. *Proc Royal Soc B* **236**:325–337. doi:10.1098/rspb.1989.0026
420 Robinson MD, McCarthy DJ, Smyth GK. 2010. edgeR: a Bioconductor package for differential expression
421 analysis of digital gene expression data. *Bioinformatics* **26**:139–140.
422 doi:10.1093/bioinformatics/btp616
423 Shinohara N, Sunagawa N, Tamura S, Yokoyama R, Ueda M, Igarashi K, Nishitani K. 2017. The plant
424 cell-wall enzyme AtXTH3 catalyses covalent cross-linking between cellulose and cello-
425 oligosaccharide. *Sci Rep* **7**:46099. doi:10.1038/srep46099
426 Shoguchi E, Shinzato C, Kawashima T, Gyoja F, Mungpakdee S, Koyanagi R, Takeuchi T, Hisata K,
427 Tanaka M, Fujiwara M, Hamada M, Seidi A, Fujie M, Usami T, Goto H, Yamasaki S, Arakaki N,
428 Suzuki Y, Sugano S, Toyoda A, Kuroki Y, Fujiyama A, Medina M, Coffroth MA, Bhattacharya
429 D, Satoh N. 2013. Draft assembly of the *Symbiodinium minutum* nuclear genome reveals
430 dinoflagellate gene structure. *Curr Biol* **23**:1399–1408. doi:10.1016/j.cub.2013.05.062
431 Sproles AE, Kirk NL, Kitchen SA, Oakley CA, Grossman AR, Weis VM, Davy SK. 2018. Phylogenetic
432 characterization of transporter proteins in the cnidarian-dinoflagellate symbiosis. *Mol Phylogenet*
433 *Evol* **120**:307–320. doi:10.1016/j.ympev.2017.12.007
434 Stat M, Morris E, Gates RD. 2008. Functional diversity in coral-dinoflagellate symbiosis. *Proc Natl Acad*
435 *Sci USA* **105**:9256–9261. doi:10.1073/pnas.0801328105
436 Sun J, Nishiyama T, Shimizu K, Kadota K. 2013. TCC: an R package for comparing tag count data with
437 robust normalization strategies. *BMC Bioinform* **14**:219. doi:10.1186/1471-2105-14-219
438 Whitehead LF, Douglas AE. 2003. Metabolite comparisons and the identity of nutrients translocated from
439 symbiotic algae to an animal host. *J Exp Biol* **206**:3149–3157. doi:10.1242/jeb.00539
440 Xiang T, Hambleton EA, DeNofrio JC, Pringle JR, Grossman AR. 2013. Isolation of clonal axenic strains
441 of the symbiotic dinoflagellate *Symbiodinium* and their growth and host specificity. *J Phycol*
442 **49**:447–458. doi:10.1111/jpy.12055
443 Xiang T, Lehnert E, Jinkerson RE, Clowez S, Kim RG, DeNofrio JC, Pringle JR, Grossman AR. 2020.
444 Symbiont population control by host-symbiont metabolic interaction in Symbiodiniaceae-
445 cnidarian associations. *Nat Commun* **11**:108. doi:10.1038/s41467-019-13963-z
446 Young MD, Wakefield MJ, Smyth GK, Oshlack A. 2010. Gene ontology analysis for RNA-seq: accounting
447 for selection bias. *Genome Biol* **11**:R14. doi:10.1186/gb-2010-11-2-r14
448
449

450 **List of figure supplements and source data files**

451 Figure 1-figure supplement 1. Effect of photosynthesis inhibitor on glucose and galactose secretion.

452 Figure 1- source data 1. Raw data of growth rates.

453 Figure 1- source data 2. Raw data of photosynthesis activities.

454 Figure 1- source data 3. Raw data of glucose and galactose concentrations.

455 Figure 2- source data 1. Raw data of bright field cell counts.

456 Figure 2- source data 2. Raw data of SEM cell counts.

457 Figure 2- source data 3. Raw data of TEM cell counts.

458 Figure 3-figure supplement 1. Mapping of DEGs between the low pH and control groups on KEGG
459 pathways.

460 Figure 3-figure supplement 2. Phylogenetic tree of the cellulase proteins.

461 Figure 3-source data 1. Expression levels of the annotated low pH DEGs.

462 Figure 3-source data 2. GO enrichment analysis results.

463 Figure 3-source data 3. CAZome analysis results.

464 Figure 3-source data 4. Multiple alignment of the cellulase proteins.

465 Figure 4- source data 1. Raw data of glucose and galactose concentrations with PSG.

466

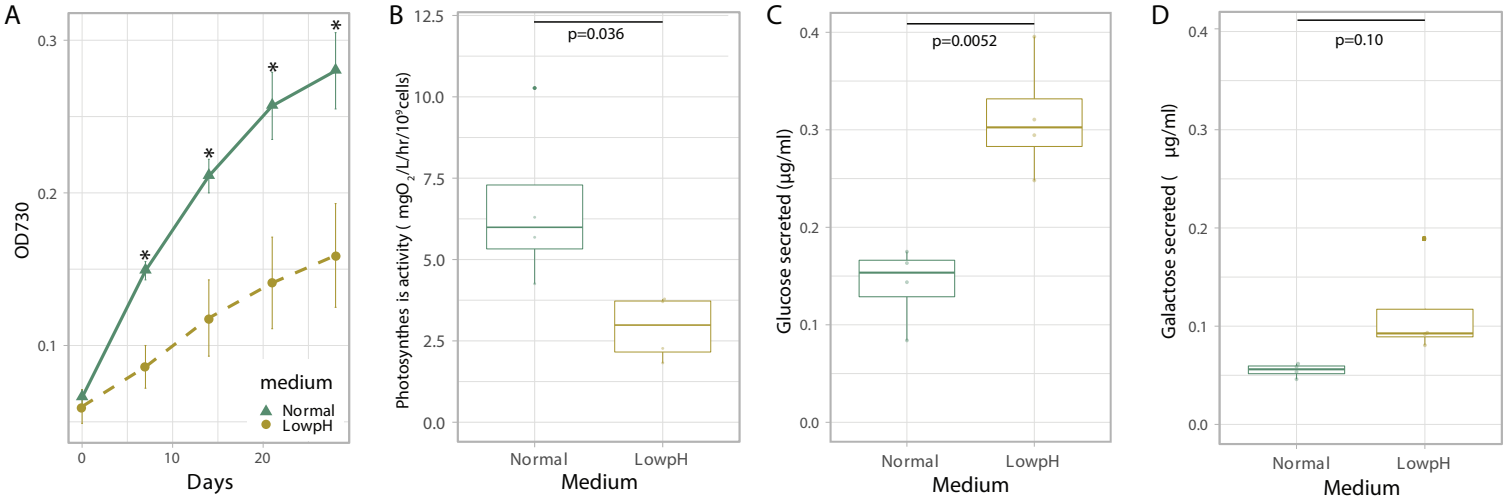

Figure 1. Physiological characterisation and monosaccharide secretion of cultured Breviolum. A. Growth rate (n = 6 per treatment, t-test). Asterisks indicate statistically significant differences (t-test, $p < 0.005$). B. Photosynthesis activity (n = 4 per treatment, t-test) C, D. Glucose (C) and galactose (D) concentrations secreted in normal and low pH media after 1 day incubation (n = 4 per treatment, t-test).

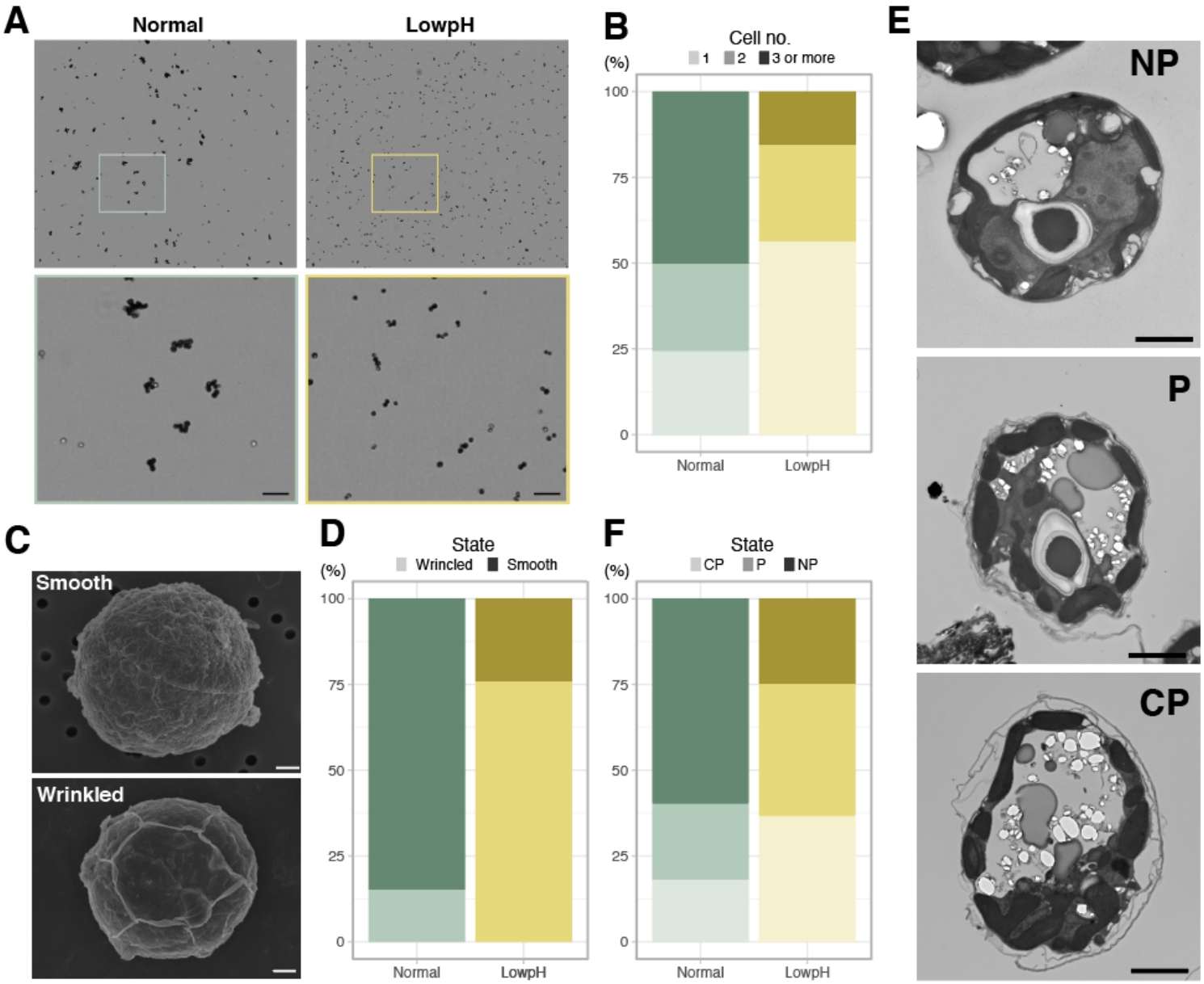

Figure 2. Cell structures under different pH condition. A. Bright field images of the cells under different conditions. The lower panels show high-magnification views of boxed areas in the upper panels. Scale bar = 50 µm. B. Quantification of the number of cells forming clusters (Fisher's exact test for "1 or 2" vs "3 or more", p = 1.727 × 10-07). C. SEM images of the representative cells. Scale bar = 1 µm. D. Quantification of the cell surface structures of the SEM images (Fisher's exact test, p < 2.2 × 10-16). E. TEM images of the representative cells. Scale bar = 2 µm. F. Quantification of the cell surface structures of the TEM images (Fisher's exact test for "P or CP" vs "NP", p = 4.621 × 10-11).

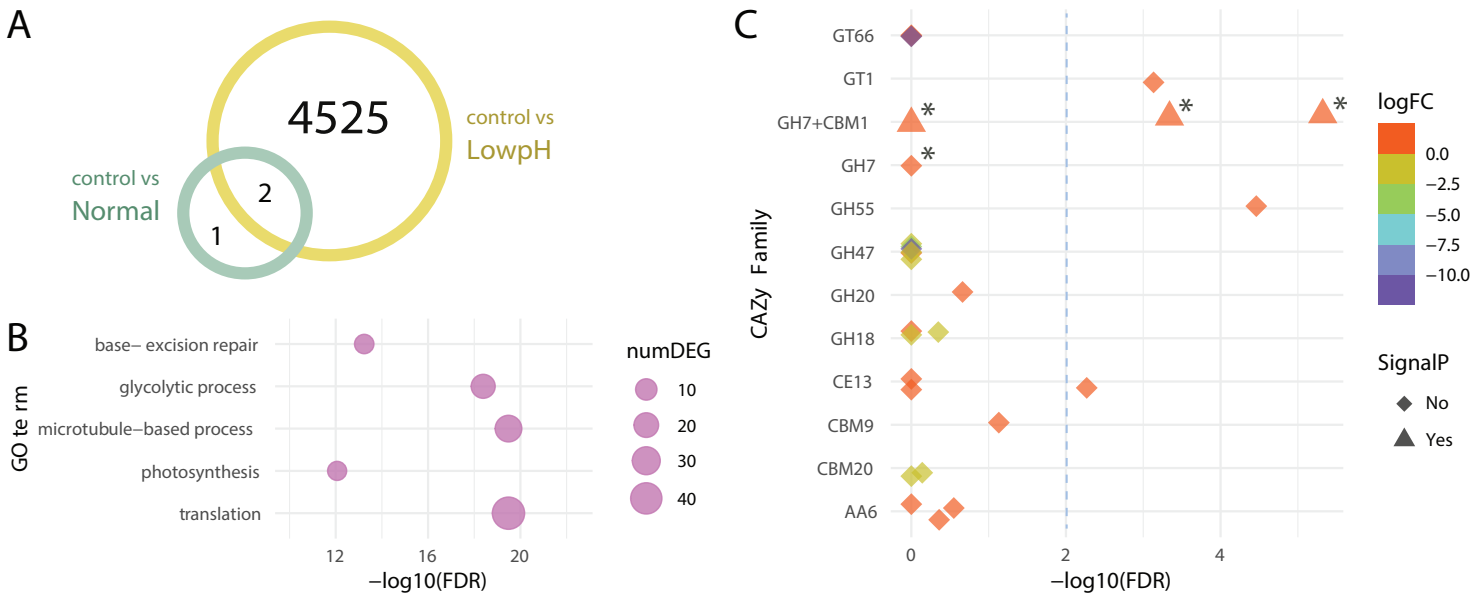

Figure 3. Differentially expressed genes under different pH conditions. A. Venn diagram showing the numbers of DEGs under different conditions. B. GO term enrichment analysis. Circles indicate the statistical significance (FDR) of the enriched GO terms, with the numbers of DEGs (numDEG) associated with each GO term. C. Isoform-level expression analysis of genes encoding CAZymes. Symbols indicate the statistical significance (FDR) of the differentially expressed isoforms associated with the DEGs, with the presence (triangle) or absence (rhombus) of signal peptide predicted in the amino acid sequence. Symbol colors represent the log fold-changes (logFC) of the expression levels of each isoform (low pH/control). Asterisks and dashed line indicate isoforms of the cellulase gene and a threshold for differential expression (FDR = 0.01), respectively.

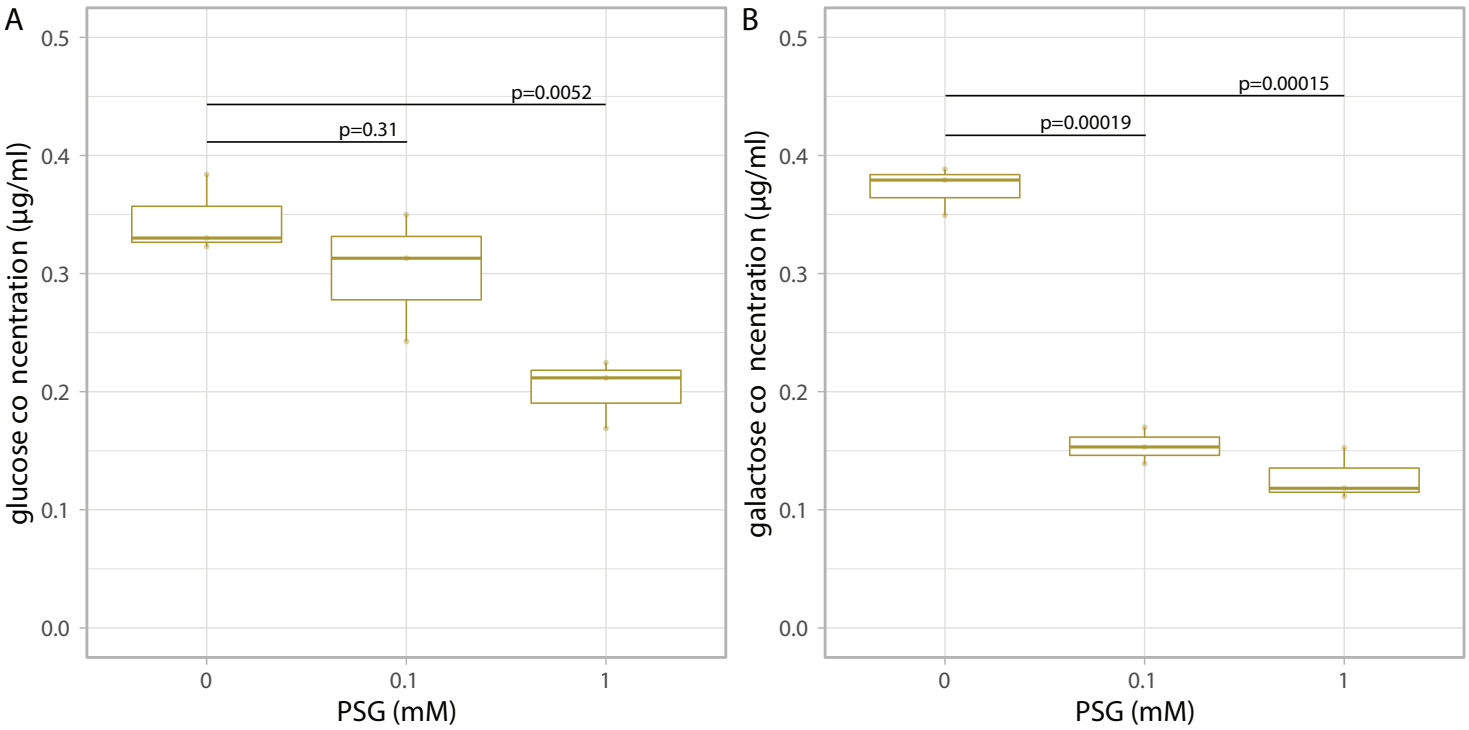

Figure 4. Glucose and galactose secretion in cellulase inhibitor treatment. The concentrations of glucose (A) and galactose (B) in the medium after 1 day incubation with PSG (n = 3 per treatment, t-test).

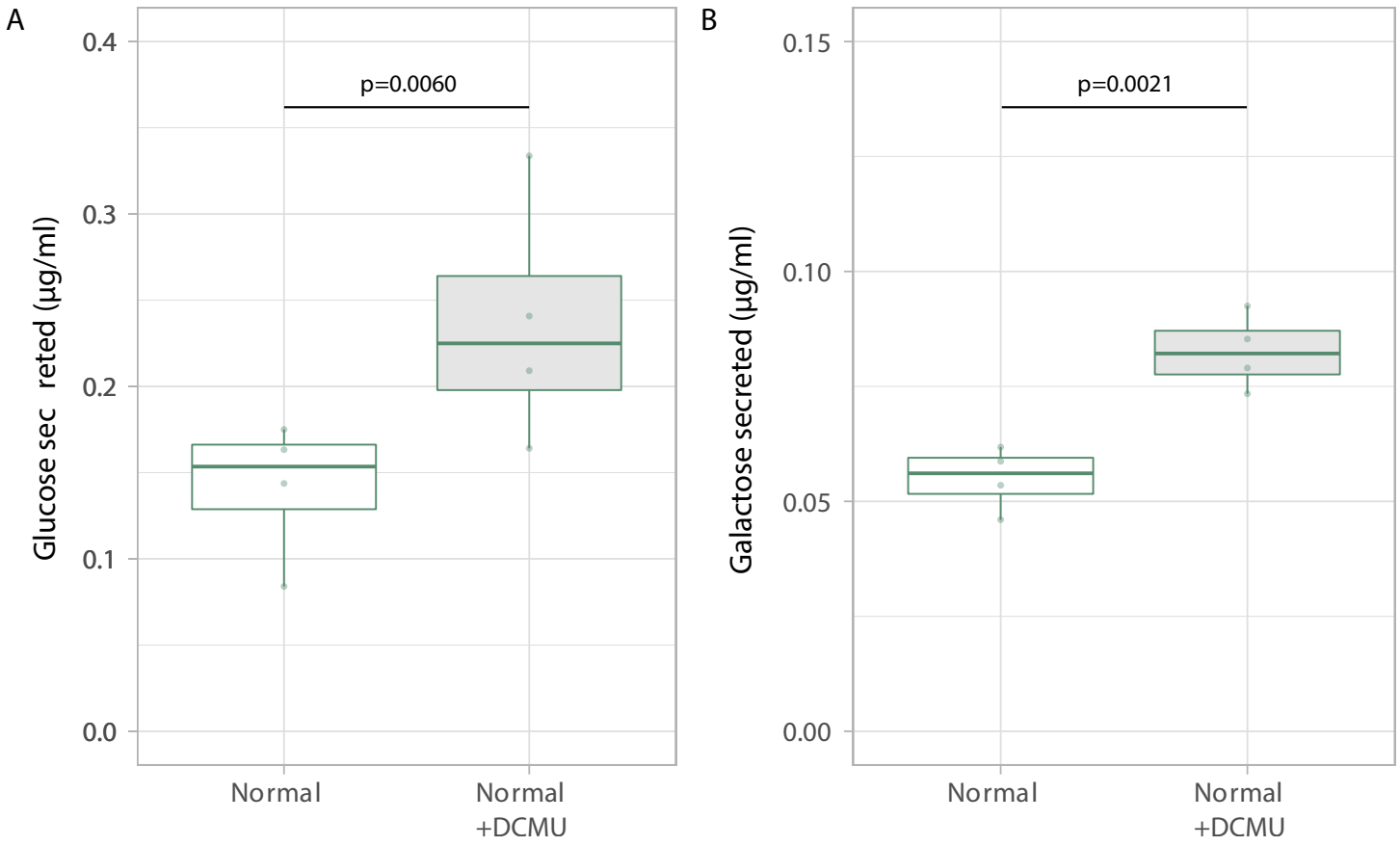

Figure 1-figure supplement 1. Effect of photosynthesis inhibitor on glucose and galactose secretion

Glucose (A) and galactose (B) secreted after 1 day incubation with and without the addition of DCMU (n = 4 per treatment, t-test). Values of 'Normal' in A were obtained from the same data shown in Figure 1.

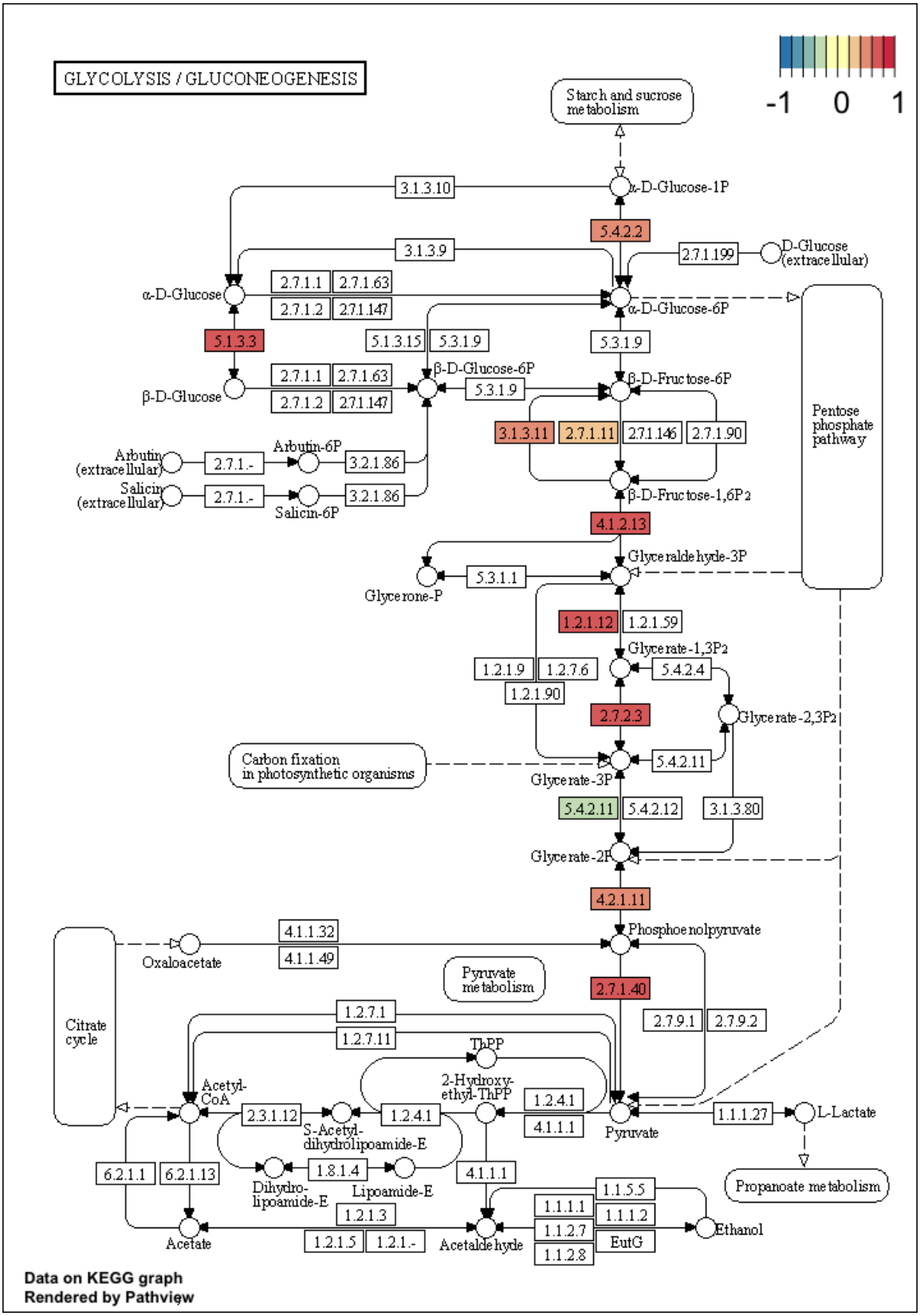

Figure 3-figure supplement 1. Mapping of DEGs between the low pH and control groups on KEGG pathways. The KEGG pathways for glycolysis/gluconeogenesis are shown. The colours indicate gene expression levels.

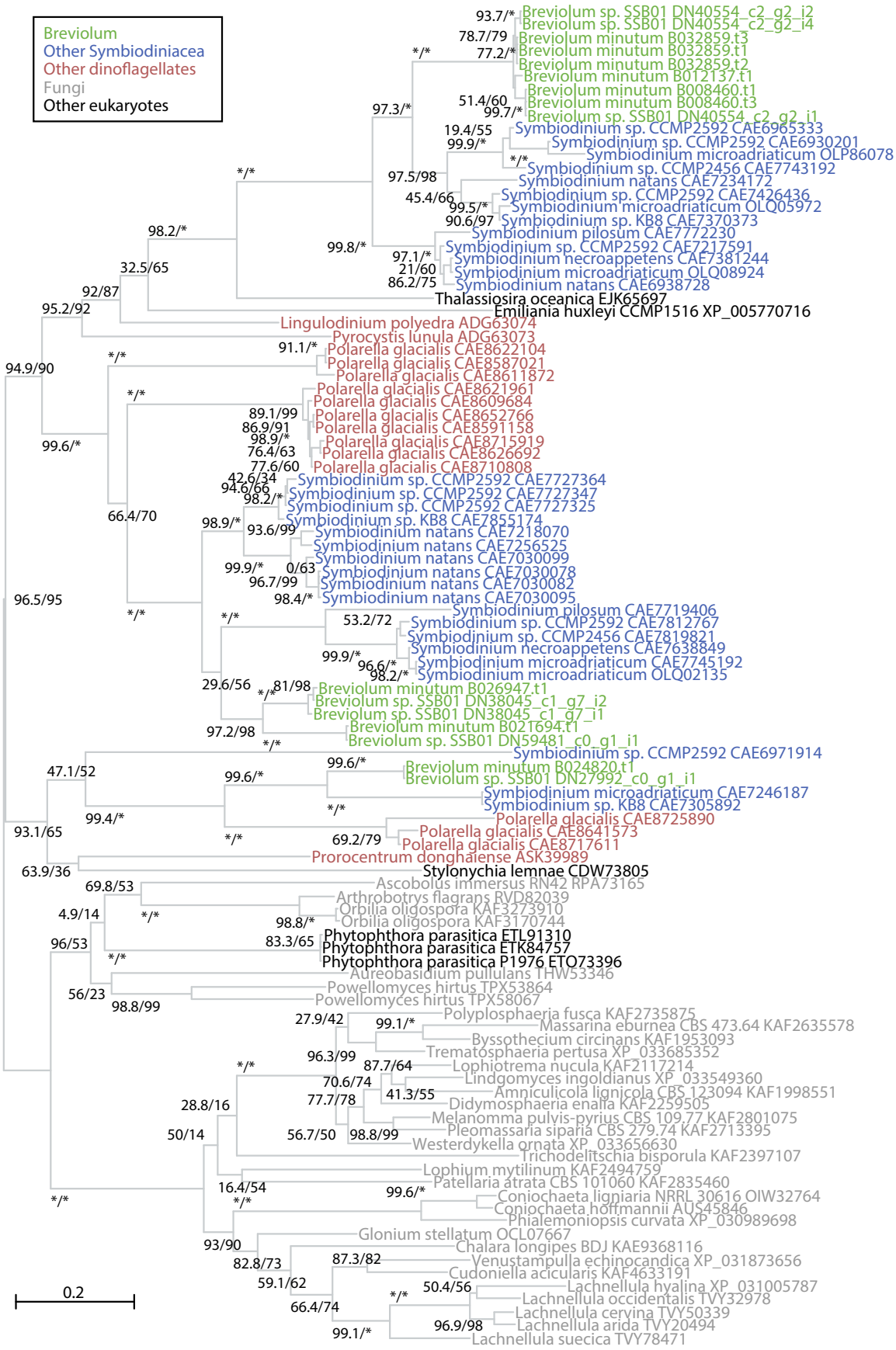

Figure 3-figure supplement 2. Phylogenetic tree of the cellulase proteins. A maximum likelihood tree of cellulase proteins labeled with species names and GenBank IDs is shown. Support values using an SH-like approximate likelihood ratio test (left) and ultrafast bootstrap approximation (right) are shown for each branch. For Breviolum sp. SSB01, the Trinity assembly contig IDs are shown.